HHS Public Access

Author manuscript

*J Biomed Nanotechnol*. Author manuscript; available in PMC 2016 October 01.

Published in final edited form as:

*J Biomed Nanotechnol*. 2015 October ; 11(10): 1836–1846.

# Biodistribution, Clearance, and Toxicology of Polymeric Micelles Loaded with 0.9 or 5 nm Gold Nanoparticles

**Ajlan Al Zaki**, **James Z. Hui**, **Elizabeth Higbee**, and **Andrew Tsourkas***

Department of Bioengineering, School of Engineering and Applied Sciences, University of Pennsylvania, Philadelphia PA, 19104, USA

## Abstract

Long-circulating gold nanoparticles (AuNPs) have garnered a great deal of interest as both imaging and therapeutic agents. However, their protracted elimination and long-term persistence within many organ systems remains a concern for clinical translation. To improve the excretion of long-circulating nanoparticles, we prepared ~80 nm biodegradable polymeric micelles with 0.9 nm or 5 nm AuNPs tightly packed within the hydrophobic core. These gold-loaded polymeric micelles (GPMs) were expected to allow for improved excretion of gold, compared with single large AuNPs, owing to the smaller size and larger surface-to-volume ratio of the individual AuNPs within the micelle. Following intravenous administration of GPMs, organs were harvested and examined for gold content using inductively coupled plasma optical emission spectrometry (ICP-OES) for up to 3 months post-injection. While both GPM formulations showed significant clearance of gold over time, micelles containing 0.9 nm AuNPs showed a 72% and 67% reduction in gold content in the liver and spleen, respectively, between 1 day and 3 months post-injection, compared with a 38% and 35% reduction in mice receiving 5 nm GPMs. Furthermore, feces and urine analysis revealed approximately 7.5 and 100 times more gold, respectively, in mice that received 0.9 nm GPMs one day after injection. These findings suggest that the excretion profile of inorganic nanomaterials may be improved if clusters of small inorganic materials are used in favor of single solid particles.

### Keywords

Gold; Nanoparticles; Biodistribution; Pharmacokinetics; Excretion; Elimination; Clearance; Toxicity

## INTRODUCTION

The use of gold nanoparticles (AuNPs) in biological applications began in 1971 when Faulk and Taylor invented the immunogold staining procedure for electron microscopy.[1] Since then, AuNPs have attracted considerable interest across a wide range of biomedical applications. For example, AuNPs have been utilized for catalysis, biosensors, cancer imaging, photothermal therapy, and drug delivery.[2,3] The widespread interest in using AuNPs for imaging and therapeutic applications stems from their ability to be finely tuned to

*Author to whom correspondence should be addressed.: atsourk@seas.upenn.edu.

many different shapes and sizes, ease of surface modification, unique optical properties, high attenuation coefficient, and the strong evidence indicating that gold is nontoxic.[4,5] In fact, aurothiolate and colloidal gold have historically been used in medical practice as a treatment for rheumatoid arthritis.[6]

Despite the beneficial aspects of using AuNPs in biomedical applications, a major lingering concern with their clinical translation is their long-term retention within many organ systems, most notably the liver and spleen. For example, it has been found that there is only a 9% drop in the content of gold in the liver from day 1 to 6 months, following the intravenous injection of 40 nm AuNPs.[7] This is consistent with a number of similar studies, which saw little to no clearance of ~20 nm AuNPs over shorter time periods (1 to 4 months).[8,9] As these inorganic particles are not readily biodegradable, they can potentially result in liver and immune system damage,[10] raising concerns about their long term toxicity and biosafety.[11,12] Previous studies have shown that whole-body clearance can be improved through the use of small AuNPs (<6 nm), since these particles are small enough to undergo glomerular filtration.[10,13,14] However, smaller AuNPs possess lower blood residence times due to their rapid renal excretion.[15] As a result, they are expected to be less favorable as blood pool agents for computed tomography (CT) angiography and for tumor targeting via enhanced permeability and retention, where nanoparticle accumulation is generally governed by blood residence time.[16,17] Moreover, larger AuNPs are also expected to be superior for receptor-targeted imaging/therapeutic studies, whereby the number of localized nanoparticles is limited by the number of cell surface receptors at the target site. Therefore, larger AuNPs would presumably allow for higher total accumulation of gold.

In this study, we examined whether a AuNP formulation could be prepared that is above the size threshold for renal clearance, but still exhibit favorable tissue clearance and excretion profiles. Specifically, we prepared ~80 nm gold-loaded polymeric micelles (GPMs) with sub-6 nm AuNPs tightly packed within the hydrophobic core (Figs. 1(A), (B)). The blood clearance profile, tissue biodistribution, and excretion of gold was evaluated over a 3 month time period. Blood chemistry as well as liver and spleen histology were also examined for indications of toxicity.

## METHODS

### Materials

PEG(4k)-b-PCL(3k) was purchased from Polymer Source (Dorval, Quebec, Canada). All other chemicals were purchased from Sigma-Aldrich (St. Louis, MO, USA) unless otherwise noted. Mice were purchased from Charles River Laboratory (Charles River, MS).

### Synthesis of 0.9 nm Gold AuNPs

Dodecanethiol-capped 0.9 nm AuNPs were prepared through the reduction of gold chloride triphenylphospine ($AuClPPh_3$) with tert-butylamine-borane ($C_4H_{14}BN$), according to the procedure described by Li et al.[18] Briefly, 0.375 mmol of $AuClPPh_3$ was added to 21 mL of ethanol at room temperature. The resultant mixture was stirred and 3.75 mmol of the tert-butylamine-borane reducing agent was added. After 30 minutes, 48 μL of dodecanethiol was

added and the dark brown solution was stirred for at least an hour. The solvent was then evaporated in a vacuum centrifuge and the particles were resuspended in toluene followed by centrifugation to remove any insoluble material. This was repeated twice.

### Synthesis of 5 nm Gold AuNPs

Dodecanethiol-capped 5 nm AuNPs were prepared using a two-phase reduction of tetrachloroaurate ($HAuCl_4$) with sodium borohydride ($NaBH_4$), followed by the addition of an alkanethiol, according to the procedure described by Brust et al.[19] Briefly, 25 mL of an aqueous solution of 35 mM hydrogen $HAuCl_4$ was mixed with 50 mM of tetraoctylammonium bromide (TOAB) in 70 mL of toluene. The solution was stirred until the $HAuCl_4$ solution transferred into the organic phase. This was followed by the drop-wise addition of a 0.4 M aqueous solution of $NaBH_4$. Then, 0.84 mM of dodecanethiol was added to the solution while stirring. The resultant mixture was then stirred for at least 3 hours and precipitated twice at −20 °C in ethanol overnight to remove excess thiols. The precipitate was collected via centrifugation and the supernatant was decanted. The remaining pellet was dissolved in toluene.

### Synthesis of GPMs

Gold-loaded polymeric micelles were synthesized using oil-in-water emulsions and stabilized using the amphiphilic diblock copolymer polyethylene glycol (4k)–polycaprolactone (3k) (PEG-*b*-PCL).[17] AuNPs, either 0.9 nm or 5 nm, were dissolved in toluene at 40 mg Au/mL and PEG-*b*-PCL was also dissolved in toluene at a concentration of 40 mg/mL. A combined solution (200 $\mu$L) of the diblock (4 mg) and the AuNPs (4 mg) was added directly to a glass vial containing 4 mL of $dH_2O$ and the mixture was emulsified for approximately 3 minutes in an ultrasonic bath. The emulsions were then allowed to stand overnight in a desiccator prior to their characterization and purification. The resulting dark brown (0.9 nm)/dark purple (5 nm) solution was centrifuged at 400 RCF for 10 minutes to remove the largest micelles. The solution was then centrifuged twice at 3100 RCF for 30 minutes, after which the supernatant was removed, and the pellet was re-suspended in pH 7.4 phosphate buffered saline (PBS). Free polymer and smaller sized particles were removed by diafiltration using a MidGee hoop cross flow cartridge with 750 kDa molecular weight cutoff (GE Healthcare, Piscataway, NJ, USA). The GPMs were then filtered through a 0.2 $\mu$m cellulose acetate membrane filter (Nalgene, Thermo Scientific) to remove any oversized particles. Finally the nanoparticles were concentrated using 50 kDa MWCO centrifugal filter units (Millipore, Billercia, MA, USA). The gold concentration was determined by inductively coupled plasma optimal emission spectroscopy (ICP-OES, Spectro Analytical Instruments GMBH; Kleve, Germany).

### Tissue Distribution and Blood Clearance

Thirty-six nude mice ($n$ = 18 per group; Charles River Laboratory, Charles River, MS) were injected intravenously under anesthesia with 75 nm GPMs (containing either 0.9 nm or 5 nm AuNPs) in PBS at dose of 150 mg Au/kg body weight. Mice were maintained in accordance with the Institutional Animal Care and Use Committee (IACUC). Mice were bled and sacrificed at various times after the injection of the agent. Specifically, three mice from each group was bled at 1 h, 2 h, 6 h, 12 h, 24 h, 3 d, 7 d, 14 d, 1 mo, and 3 mo, and the blood

collected and analyzed for gold by ICP-OES. Each mouse was bled twice. Therefore, 10 uL blood samples were collected via the tail-nick method from three animals at the following times: 1 hour and 3 days, 2 hours and 7 days, 6 hours and 14 days, 24 hours and 1 month, and 1 hour and 3 months. At the second bleed time point, the mice were euthanized by $CO_2$ and 0.3 mL blood was removed by cardiac puncture from the right ventricle immediately after the cessation of breathing. After the final aliquot of blood was collected the brain, heart, lungs, kidneys, spleen, liver, skin, small bowel, large bowel, pancreas, thyroid, femur, and inguinal lymph nodes were removed from each animal. Three additional mice per GPM formulation were used for three additional blood collections at 5 minutes, 10 minutes, and 15 minutes and sacrificed at 24 hours and organs harvested. Organ samples were washed with PBS to minimize contamination from any nanoparticles still circulating in the blood. The blood samples and organs were then analyzed for gold content by ICP-OES. Organ samples were weighed into Teflon PFA vials (Savillex, Minnetonka, MN, USA) and digested overnight at 60 °C with 70% nitric acid to digest the organic material. HCl was added the next day and the digest continued to dissolve the inorganic material. Blood samples were dissolved directly in aqua regia. Blood GPM content was calculated as the percent of the injected dose per gram of blood analyzed (%ID/g). Organ GPM content was similarly calculated as the percent of the injected dose present per gram of tissue.

## Toxicity Studies

Blood samples obtained by cardiac puncture were analyzed for blood chemistry analytes (alanine aminotransferase (ALT), aspartate aminotransferase (AST), alkaline phosphatase, and total bilirubin (TBIL). All samples were analyzed by the diagnostic core laboratories at the University of Pennsylvania School of Veterinary Medicine.

## Hematoxylin and Eosin (H&E) Staining

Hematoxylin-eosin (HE) staining was performed using 5 $\mu$m thickness sections from formalin-fixed, paraffin-embedded tissue blocks. Specimens were fixed in formalin (Fisher Scientific, Waltham, MA) immediately after harvesting and followed by gradient dehydration with 70%, 95%, and 100% ethanol. Tissue were then processed in xylene (Fisher) and embedded in paraplast tissue embedding medium (Fisher). Slides were prepared using Microm HM550. Paraffin sections were deparaffinized in xylene followed by rehydration with 100%, 95%, 70% ethanol and then Milli-Q water (Millipore, Bedford, MA) before the staining. Harris hematoxylin (Fisher) was used for nuclei staining. Excess hematoxylin was removed by dipping slides in acid alcohol (Leica Biosystems, Richmond, VA). Slides were then placed in running warm water until the nuclei turned blue. Eosin (Leica Biosystems) was used to stain for cytoplasm. Slides were later mounted using permount (Fisher) after clearing with xylene.

## Numerical and Statistical Analysis

All numerical and statistical analysis was performed in Microsoft Excel. Where appropriate, a Student's *t*-test was used to determine if differences were statistically significant. Measurements of AuNP size were reported as mean±standard deviation. All other error bars are reported as standard error of the mean.

# RESULTS

## Characterization of 0.9 and 5 nm AuNPs

To prepare GPMs with 0.9 nm or 5 nm AuNPs encapsulated within the hydrophobic core (Figs. 1(A), (B)), hydrophobic AuNPs were synthesized with dodecanethiol as a capping agent. The AuNPs had a low polydisperity and diameters of 0.93±0.19 and 4.66±0.57 nm, respectively, according to an analysis of transmission electron microscopy (TEM) images (Fig. 2 and Table I). Purity was further confirmed via UV–vis spectroscopy (Fig. 2).

## Synthesis and Characterization of GPMs

GPMs were prepared by encapsulating either 0.9 or 5 nm AuNPs within the hydrophobic core of a polymeric micelle, using an oil-in-water microemulsion method.[17] The polymeric micelle was formed using the biodegradable amphiphilic diblock copolymer, PEG-b-PCL. The GPMs were soluble in aqueous solutions owing to the hydrophilic PEG corona of the diblock copolymer. Following synthesis and purification of the GPMs, ~80 nm GPMs were isolated using differential centrifugation, as confirmed by dynamic light scattering (DLS) (Fig. 1(C)). The DLS measurements demonstrate particle measurements with a low polydispersity index for both GPM formulations (< 0.1). TEM micrographs revealed that the GPMs were spherical with tightly packed clusters of AuNPs within the hydrophobic core of the micelles (Figs. 1(D), (E)). The zeta potential of the two GPM formulations was near neutral. A summary of the GPM physical-chemical properties is provided in Table I.

## GPM Pharmacokinetics

Following intravenous administration, 0.9 and 5 nm GPMs exhibited similar blood clearance profiles with circulation half-lives of ~1.5 hours and ~2.6 hours, respectively (Fig. 3). The biodistribution of GPMs was evaluated at 1 day, 3 days, 1 week, 2 weeks, 1 month, and 3 months post-injection (150 mg Au/kg) by performing an inductively coupled plasma–optical emission spectroscopy (ICP-OES) analysis of gold content within the brain, thyroid, lungs, heart, liver, spleen, small bowel, large bowel, kidneys, pancreas, sublingual lymph nodes, skin, bone, muscles, feces, and urine. As expected, the largest fractions of gold were observed in the spleen and liver (Fig. 4).

Higher levels of gold were observed in the spleen following intravenous injection of the 5 nm GPMs, compared with the 0.9 nm GPMs, for all time points studied. However, both groups showed a marked reduction in gold accumulation between one day and three months post-injection. Specifically, there was a 35% reduction of gold in the spleen of mice that received 5 nm GPMs and a 55% reduction of gold in the spleen of mice that received 0.9 nm GPMs.

Initially, the levels of Au within the liver were higher for the 0.9 nm GPM group (40.3±6.3% ID/g), compared with the 5 nm GPM group (23.7±2.5% ID/g). However, after 3 months the Au content dropped more dramatically in mice that received the 0.9 nm GPMs (65%) compared to the 5 nm GPMs (38%). As a result, the 0.9 nm GPM group (14.3 ± 1.5% ID/g) and 5 nm GPM group (14.7±1.4% ID/g) had similar levels of gold retained in the liver at this later time point.

Hepatobiliary excretion appeared to be the primary pathway for gold removal, with measureable levels of gold detected in the feces following injection of both 0.9 nm and 5 nm GPMs. However, this excretion pathway appeared to be significantly more efficient for the 0.9 nm GPMs, compared to the 5 nm GPMs, with approximately 7.5 times more gold detected in the feces one day post-injection. For both groups, the gold content in the feces decreased over the duration of the study with no detectable levels at 3 months.

Consistent with the more efficient removal of gold from 0.9 nm GPMs via the hepatobiliary system, qualitatively higher levels of gold were also found in the small bowel, although not statistically significant, one day and 3 days post-injection, compared with mice receiving 5 nm GPMs. By one week and at all subsequent time points, similar levels of gold were observed in the small bowels for both GPM formulations. Evidence of hepatobiliary excretion is consistent with previous studies, which have shown that AuNPs that are taken up by Kupffer cells and hepatocytes are secreted primarily by hepatocytes within the first 24 hours through the hepatobiliary pathway, after which they are cleared through Kupffer cells through mechanisms that are poorly understood.[20, 21]

The quantity of gold found in the kidneys was far lower than what was found in the liver and spleen for both the 0.9 nm and 5 nm GPM groups. This is not surprising considering that GPMS are too large to undergo glomerular filtration. It was anticipated that the GPMs would be predominantly taken up by the reticuloendothelial system (RES) prior to breakdown of the polymeric micelle and release of the encapsulated AuNPs. Nonetheless, a measureable amount of gold was detected in the kidneys, with statistically significant lower levels of gold found one day, 1 month and 3 months post-injection of the 0.9 nm GPMs, compared with 5 nm GPMs. This difference was most pronounced at the later two time points. Interestingly, there also seemed to be some renal excretion of gold from mice that received 0.9 nm GPMs. In fact, approximately 100-fold more gold was detected in the urine one day following the administration of 0.9 nm GPMs (0.29% ID/g) compared with 5 nm GPMs (0.003% ID/g). These urine concentrations gradually decreased to undetectable levels at 3 months. We attribute the difference between the two GPM formulations to be a direct result of the difference in the sizes of encapsulated AuNPs. Since 0.9 nm AuNPs are much smaller than the size cut-off limit for successful glomerular filtration, even if opsonized, they should enjoy more efficient excretion into the urine than the larger 5 nm AuNPs.

Two organs that appeared to exhibit somewhat surprising levels of gold following the injection of the 5 nm GPMs were the brain and heart (Fig. 5). Specifically, in the brain we detected 2.8±0.3% ID/g one day post-injection, compared with only 0.14±0.03% ID/g for 0.9 nm GPMs. Although not high per se, this level of gold is readily measureable. Nonetheless, it is likely that gold from the 5 nm GPMs did not penetrate the blood-brain barrier considering their large size and that levels of gold were at or near the detection limit after just one week post-injection. Gold would presumably not be cleared from brain in such a short timeframe if it has entered the brain parenchyma. The presence of gold does not seem to be an artifact since it was found to be at similar levels in all of the mice at one and three days post-injection. Notably, others have also reported the presence of low levels of AuNPs (15 nm and 50 nm) in brain 24 hrs after intravenous injection.[22]

In the heart, the gold content was 2 times greater one day following the administration of 5 nm GPMs (3.1 ± 0.2% ID/g) compared with 0.9 nm GPMs (1.5±.06% ID/g). Both groups showed a reduction in gold content (75% for 5 nm GPMs and 86% for 0.9 nm GPMs) in the heart over 3 months, however, mice receiving 5 nm GPMs possessed higher levels of gold at all time points.

In the skin, the gold content fluctuated between 2 and 12% ID/g (on average) during the duration of the studies with no statistically significant differences between the 0.9 nm and 5 nm GPMs during the 3 month time period (Fig. 6). The skin has long been shown to be an important site of accumulation for nanoparticles that are administered intravenously. Studies have shown that AuNPs can exit blood vessels in the skin and be phagocytosed by dermal macrophages and dendritic cells.[23] As these phagocytes become saturated they begin to accumulate in the pericellular space of the dermis and subcutaneous tissue. In fact, this phenomenon was visible in the skin of mice injected with GPMs, which did have some discoloration. The distribution of GPMs in the skin of mice was heterogeneous with some areas exhibiting a dark purplish hue and other areas showing little to no change in skin color.

High overall levels of gold were also observed in the lymph nodes of mice following the injection of 0.9 nm and 5 nm GPMs, with levels exceeding 20% ID/g at various time points for both groups (Fig. 6). However, due to the high variability, no statistically significant differences were observed between the groups at any one time point. High lymph uptake was not completely unexpected considering that many studies have shown the accumulation of nanomaterials in lymph nodes, in the size range of 10–300 nm.[23–28] It has been postulated that nanomaterials can slowly extravasate from the vascular to interstitial space, and are then transported to lymph nodes through the lymphatic vessels. Alternatively, it has also been suggested that nanoparticles can be taken up by the RES and trafficked to the lymph nodes.

For most of the other organs that were examined, including the thyroid, pancreas, large bowel, and muscle, there was a general trend of higher levels of gold in mice injected with 5 nm GPMs, compared with 0.9 nm GPMs (Fig. 7). However, at most time points the differences were not statistically different and the overall levels of gold were quite low, < 2.5% ID/g (on average). Both groups showed a significant reduction in gold content over the 3-month time period in each of these organs.

In bone, the levels of gold were generally higher in mice receiving 0.9 nm GPMs, particularly at early time points, but again the differences were not statistically significant (Fig. 7). Similar levels of gold were observed in the lungs following the injection of 0.9 nm and 5 nm GPMs for all time points (Fig. 7). A significant reduction in gold was observed in both bone and lungs following the injection of 0.9 nm and 5 nm GPMs.

## Toxicity Analysis

The intravenous injection of 0.9 nm and 5 nm GPMs into healthy mice led to no signs of illness, change in activity, or weight loss (Fig. 8). A toxicological analysis of mice 1 day, 1 week, 1 month and 3 months following the administration of GPMs revealed blood chemistry levels within normal limits, despite being highly variable (Fig. 9). It should be noted that enzyme levels can fluctuate due to the method and rate of blood collection, time

of day in which blood was collected, and level of animal physical activity and are therefore highly variable in nature.[23]

### Histology of Liver and Spleen

To further evaluate the potential toxicity of GPMs, histological analysis was performed on the liver and spleen 1 day, 1 week, 1 month, and 3 months following the injection of 0.9 nm and 5 nm GPMs. Hematoxylin and eosin (H&E) stains of these organs showed no evidence of abnormal pathology or adverse effects (Fig. 10). These results are consistent with previously established literature touting the safety profile of AuNPs.[11, 29–34]

## DISCUSSION

Numerous reports have indicated that AuNPs are poorly cleared from the reticuloendothelial system following intravenous administration. For example, Balasubramanian et al. showed that in rats injected with 20 nm PEG AuNPs, gold levels in the liver and spleen remain high even at 2 months follow up–only a 6% reduction in gold.[8] In another study by Sadauskas et al., analysis of livers in mice injected with 40 nm AuNPs resulted in only a modest 9% reduction in gold content over a 6-month time period.[7] Goel et al. found that the gold content in the liver was reduced by approximately 50% following the injection of 33 nm PEG AuNPs, but that levels of gold in the spleen remained essentially unchanged 3 months post-injection.[9] In this study we investigated the organ distribution and retention of GPMs, which consist of clusters of 0.9 or 5 nm AuNPs encapsulated within the hydrophobic micelle core, for up to three months post-injection. As expected, accumulation was highest in organs rich in macrophages (liver, spleen, lymph nodes). However, in contrast to the many studies that report inefficient clearance and a persistent accumulation of AuNPs within the reticuloendothelial system, we observed a 65% and 55% reduction in gold content in the liver and spleen, respectively, between 1 day and 3 months following the injection of 0.9 nm GPMs. A 38% and 35% reduction in gold content was observed in the liver and spleen, respectively, following injection of 5 nm GPMs. A reduction of gold in most other organs was observed as well. The primary mechanism of excretion seemed to be via the hepatobiliary systems, although some renal clearance was also observed. In general, GPMs containing 0.9 nm AuNPs seemed to exhibit more efficient excretion compared to 5 nm GPMs, with higher levels of gold detected in the feces and urine at earlier time points (1–7 days).

After GPMs are phagocytosed by reticuloendothelial cells, it is not clear whether the AuNPs undergo some level of dissolution, following hydrolysis of the polymeric micelle, or if they remain intact. The absence of any gold from the 5 nm AuNPs in the urine suggests little to no dissolution of this formulation. It is more likely that the 5 nm AuNPs, or clusters of 5 nm AuNPs, were secreted directly into the bile. The 0.9 nm AuNPs were perhaps more susceptible to dissolution, but no definitive conclusion can be drawn because, even if intact, they are much smaller than the size cut-off limit for glomerular filtration. Therefore, either mechanism remains possible.

Another related question is whether the individual AuNPs remain clustered within lysosomes, following phagocytosis and hydrolysis of the polymeric micelle. After all, the

AuNPs are hydrophobic in nature and initially exist as a tightly packed cluster within the hydrophobic core of the micelles. The retention of large AuNP clusters within lysosomes would be consistent with the incomplete excretion that was observed, since these clusters would effectively behave as single solid gold nanoparticles. Of course, since some improvement in excretion was observed, it is hypothesized that at least some of the AuNPs or small clusters of AuNPs become dispersed. Otherwise, no improvement in excretion would be expected. The AuNPs may have become dispersed as a result of opsonization and the formation of a thin, water-soluble protein corona. This could explain how at least some of the 0.9 nm AuNPs were able to undergo renal clearance.

## CONCLUSIONS

Overall, these findings suggest that the excretion profile of inorganic nanomaterials may be improved if nanoparticles formed from clusters of small inorganic materials are used in favor of single solid particles. For GPMs, the extent of excretion seems to correlate inversely with the size of the encapsulated AuNPs, but excretion remained incomplete for both the 0.9 and 5 nm GPMs over a 3 month period. Nonetheless, both the 0.9 nm and 5 nm GPMs were found to be biocompatible with no evidence of toxicity as measured by blood chemistry, loss in body weight, signs of distress, and histological analysis of liver and spleen tissue sections. Notably, GPMs have already been shown to be effective as both radiosensitizers and CT contrast agents.[17] Therefore, GPMs may represent a viable option for both therapeutic and/or diagnostic applications.

## Acknowledgments

The authors gratefully acknowledge Dewight Williams for assistance with the TEM and David Vann for help with ICP-OES. This work was supported by NIH/NIBIB (R21EB013754 and R01EB012065) and NIH/NCI (R01CA157766 and R01CA181429).

## References

1. Faulk WP, Taylor GM. An immunocolloid method for the electron microscope. Immunochemistry. 1971; 8:1081. [PubMed: 4110101]
2. Ulijn RV, Smith AM. Designing peptide based nanomaterials. Chem Soc Rev. 2008; 37:664. [PubMed: 18362975]
3. Giljohann DA, Seferos DS, Daniel WL, Massich MD, Patel PC, Mirkin CA. Gold nanoparticles for biology and medicine. Angew Chem Int Ed Engl. 2010; 49:3280. [PubMed: 20401880]
4. Jeremic B, Aguerri AR, Filipovic N. Radiosensitization by gold nanoparticles. Clin Transl Oncol. 2013; 15:593. [PubMed: 23359187]
5. Dorsey JF, Sun L, Joh DY, Witztum A, Al Zaki A, Kao GD, Alonso-Basanta M, Avery S, Tsourkas A, Hahn SM. Gold nanoparticles in radiation research: Potential applications for imaging and radiosensitization. Transl Can Res. 2013; 2
6. Hebert EM, Debouttiere PJ, Lepage M, Sanche L, Hunting DJ. Preferential tumour accumulation of gold nanoparticles, visualised by Magnetic Resonance Imaging: Radiosensitisation studies *in vivo* and *in vitro*. Int J Radiat Biol. 2010; 86:692. [PubMed: 20586540]
7. Sadauskas E, Danscher G, Stoltenberg M, Vogel U, Larsen A, Wallin H. Protracted elimination of gold nanoparticles from mouse liver. Nanomedicine. 2009; 5:162. [PubMed: 19217434]
8. Balasubramanian SK, Jittiwat J, Manikandan J, Ong CN, Yu LE, Ong WY. Biodistribution of gold nanoparticles and gene expression changes in the liver and spleen after intravenous administration in rats. Biomaterials. 2010; 31:2034. [PubMed: 20044133]

9. Goel R, Shah N, Visaria R, Paciotti GF, Bischof JC. Biodistribution of TNF-alpha-coated gold nanoparticles in an *in vivo* model system. Nanomedicine (Lond). 2009; 4:401. [PubMed: 19505243]
10. De Jong WH, Hagens WI, Krystek P, Burger MC, Sips AJ, Geertsma RE. Particle size-dependent organ distribution of gold nanoparticles after intravenous administration. Biomaterials. 2008; 29:1912. [PubMed: 18242692]
11. Lewinski N, Colvin V, Drezek R. Cytotoxicity of nanoparticles. Small. 2008; 4:26. [PubMed: 18165959]
12. Shichibu Y, Negishi Y, Tsukuda T, Teranishi T. Large-scale synthesis of thiolated Au25 clusters via ligand exchange reactions of phosphine-stabilized Au11 clusters. J Am Chem Soc. 2005; 127:13464. [PubMed: 16190687]
13. Sadauskas E, Wallin H, Stoltenberg M, Vogel U, Doering P, Larsen A, Danscher G. Kupffer cells are central in the removal of nanoparticles from the organism. Part Fibre Toxicol. 2007; 4:10. [PubMed: 17949501]
14. Semmler-Behnke M, Kreyling WG, Lipka J, Fertsch S, Wenk A, Takenaka S, Schmid G, Brandau W. Biodistribution of 1.4-and 18-nm gold particles in rats. Small. 2008; 4:2108. [PubMed: 19031432]
15. Hainfeld JF, Slatkin DN, Focella TM, Smilowitz HM. Gold nanoparticles: A new X-ray contrast agent. Br J Radiol. 2006; 79:248. [PubMed: 16498039]
16. Tam JM, Tam JO, Murthy A, Ingram DR, Ma LL, Travis K, Johnston KP, Sokolov KV. Controlled assembly of biodegradable plasmonic nanoclusters for near-infrared imaging and therapeutic applications. ACS Nano. 2010; 4:2178. [PubMed: 20373747]
17. Al Zaki A, Joh D, Cheng Z, De Barros AL, Kao G, Dorsey J, Tsourkas A. Gold-loaded polymeric micelles for computed tomography-guided radiation therapy treatment and radiosensitization. ACS Nano. 2014; 8:104. [PubMed: 24377302]
18. Li Y, Liu S, Yao T, Sun Z, Jiang Z, Huang Y, Cheng H, Jiang Y, Xie Z, Pan G, Yan W, Wei S. Controllable synthesis of gold nanoparticles with ultrasmall size and high monodispersity via continuous supplement of precursor. Dalton Trans. 41:11725. [PubMed: 22903561]
19. Brust M, Walker M, Bethell D, Schiffrin DJ, Whyman R. Synthesis of thiol-derivatized gold nanoparticles in a 2-phase liquid–liquid system. J Chem Soc Chem Commun. 1994; 801
20. Hardonk MJ, Harms G, Koudstaal J. Zonal heterogeneity of rat hepatocytes in the *in vivo* uptake of 17 nm colloidal gold granules. Histochemistry. 1985; 83:473. [PubMed: 4077586]
21. Paciotti GF, Myer L, Weinreich D, Goia D, Pavel N, McLaughlin RE, Tamarkin L. Colloidal gold: A novel nanoparticle vector for tumor directed drug delivery. Drug Deliv. 2004; 11:169. [PubMed: 15204636]
22. Sonavane G, Tomoda K, Makino K. Biodistribution of colloidal gold nanoparticles after intravenous administration: Effect of particle size. Colloids Surf B Biointerfaces. 2008; 66:274. [PubMed: 18722754]
23. Sykes EA, Dai Q, Tsoi KM, Hwang DM, Chan WC. Nanoparticle exposure in animals can be visualized in the skin and analysed via skin biopsy. Nat Commun. 2014; 5:3796. [PubMed: 24823347]
24. Weissleder R, Nahrendorf M, Pittet MJ. Imaging macrophages with nanoparticles. Nat Mater. 2014; 13:125. [PubMed: 24452356]
25. Harisinghani MG, Barentsz J, Hahn PF, Deserno WM, Tabatabaei S, van de Kaa CH, de la Rosette J, Weissleder R. Noninvasive detection of clinically occult lymph-node metastases in prostate cancer. N Engl J Med. 2003; 348:2491. [PubMed: 12815134]
26. Thorek DL, Ulmert D, Diop NF, Lupu ME, Doran MG, Huang R, Abou DS, Larson SM, Grimm J. Non-invasive mapping of deep-tissue lymph nodes in live animals using a multimodal PET/MRI nanoparticle. Nat Commun. 2014; 5:3097. [PubMed: 24445347]
27. Garnett MC, Kallinteri P. Nanomedicines and nanotoxicology: Some physiological principles. Occup Med (Lond). 2006; 56:307. [PubMed: 16868128]
28. Oh MH, Lee N, Kim H, Park SP, Piao Y, Lee J, Jun SW, Moon WK, Choi SH, Hyeon T. Large-scale synthesis of bioinert tantalum oxide nanoparticles for X-ray computed tomography imaging and bimodal image-guided sentinel lymph node mapping. J Am Chem Soc. 2011; 133:5508. [PubMed: 21428437]

29. Tkachenko AG, Xie H, Coleman D, Glomm W, Ryan J, Anderson MF, Franzen S, Feldheim DL. Multifunctional gold nanoparticle-peptide complexes for nuclear targeting. J Am Chem Soc. 2003; 125:4700. [PubMed: 12696875]

30. Shukla R, Bansal V, Chaudhary M, Basu A, Bhonde RR, Sastry M. Biocompatibility of gold nanoparticles and their endocytotic fate inside the cellular compartment: A microscopic overview. Langmuir. 2005; 21:10644. [PubMed: 16262332]

31. Pan Y, Neuss S, Leifert A, Fischler M, Wen F, Simon U, Schmid G, Brandau W, Jahnen-Dechent W. Size-dependent cytotoxicity of gold nanoparticles. Small. 2007; 3:1941. [PubMed: 17963284]

32. Connor EE, Mwamuka J, Gole A, Murphy CJ, Wyatt MD. Gold nanoparticles are taken up by human cells but do not cause acute cytotoxicity. Small. 2005; 1:325. [PubMed: 17193451]

33. Chen PC, Mwakwari SC, Oyelere AK. Gold nanoparticles: From nanomedicine to nanosensing. Nanotechnol Sci Appl. 2008; 1:45. [PubMed: 24198460]

34. Lasagna-Reeves C, Gonzalez-Romero D, Barria MA, Olmedo I, Clos A, Sadagopa Ramanujam VM, Urayama A, Vergara L, Kogan MJ, Soto C. Bioaccumulation and toxicity of gold nanoparticles after repeated administration in mice. Biochem Biophys Res Commun. 2010; 393:649. [PubMed: 20153731]

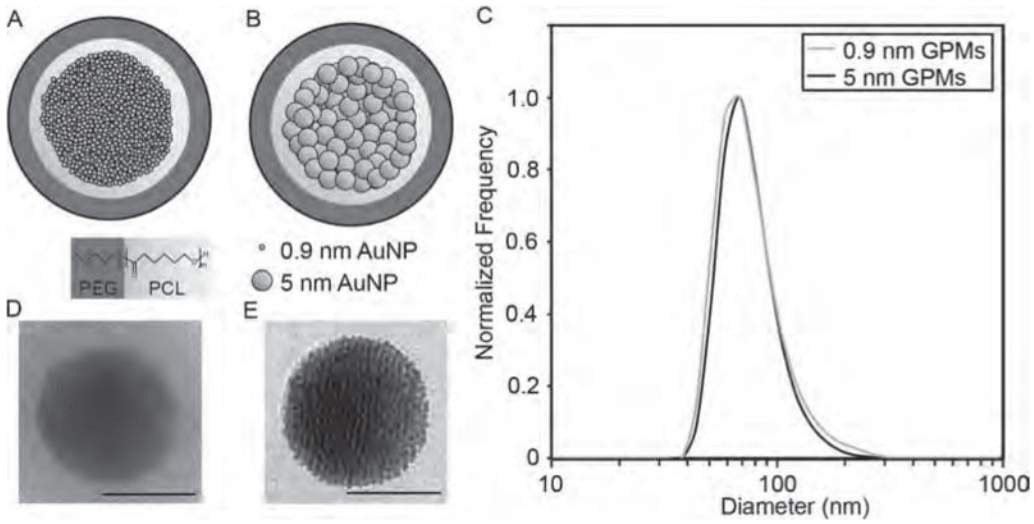


**Figure 1.**

Schematic and size analysis of GPMs. Schematic of (A) 0.9 nm GPMs and (B) 5 nm GPMs. Both GPM formulations consist of AuNPs encapsulated within the hydrophobic core of micelles formed using the biodegradable diblock co-polymer PEG-b-PCL. (C) Dynamic light scattering profiles of 0.9 nm and 5 nm GPMs. Representative transmission electron microscopy (TEM) images of a (D) 0.9 nm and (E) 5 nm GPM. All scale bars = 50 nm.

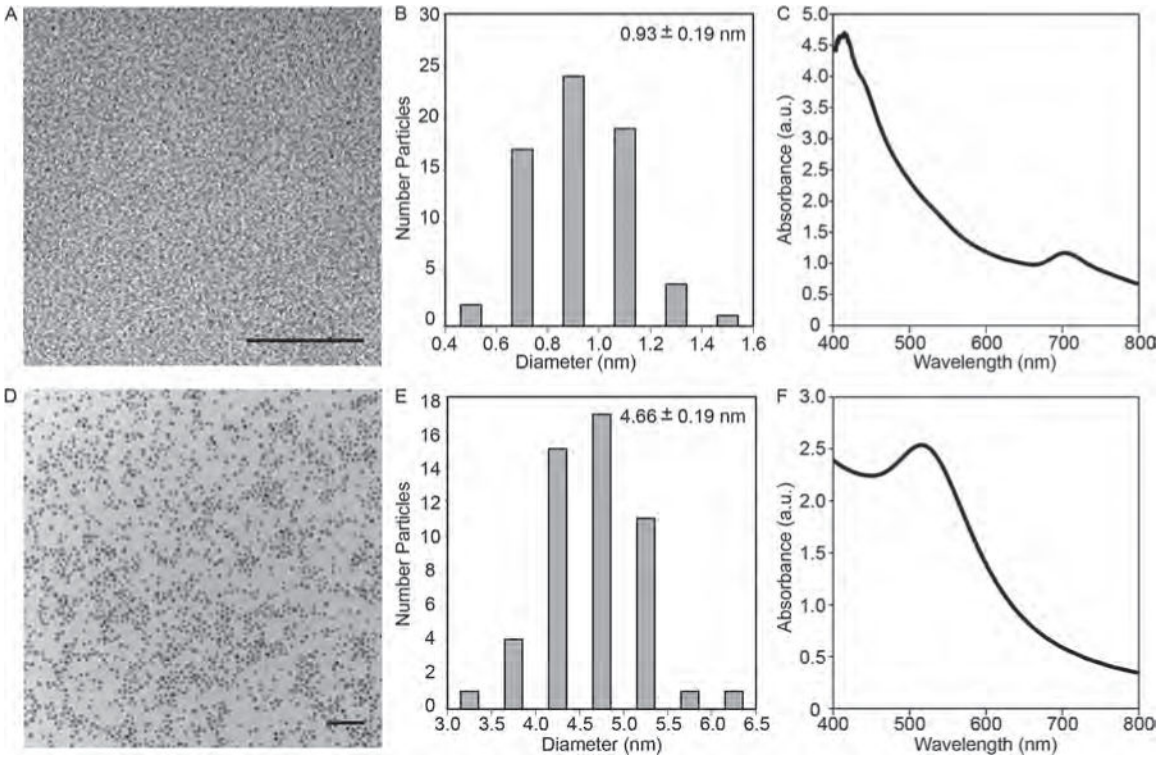


**Figure 2.**

(A) Transmission electron micrograph of 0.9 nm AuNPs. Scale bar = 20 nm. (B) Core size distribution of 0.9 nm AuNPs. The mean size and standard deviation is shown. (C) UV-vis absorption spectrum of 0.9 nm AuNPs. (D) Transmission electron micrograph of 5 nm AuNPs. Scale bar = 50 nm. (E) Core size distribution of 5 nm AuNPs. The mean size and standard deviation is shown. (F) UV-vis absorption spectrum of 5 nm AuNPs.

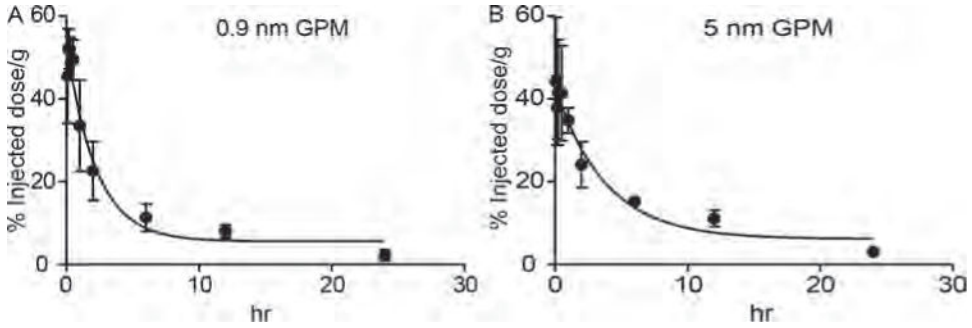


**Figure 3.**

Blood clearance profiles of GPMs. The amount of gold content in circulation was measured by ICP-OES at various times following the intravenous administration of (A) 0.9 nm GPMs and (B) 5 nm GPM in mice ($n = 3$).

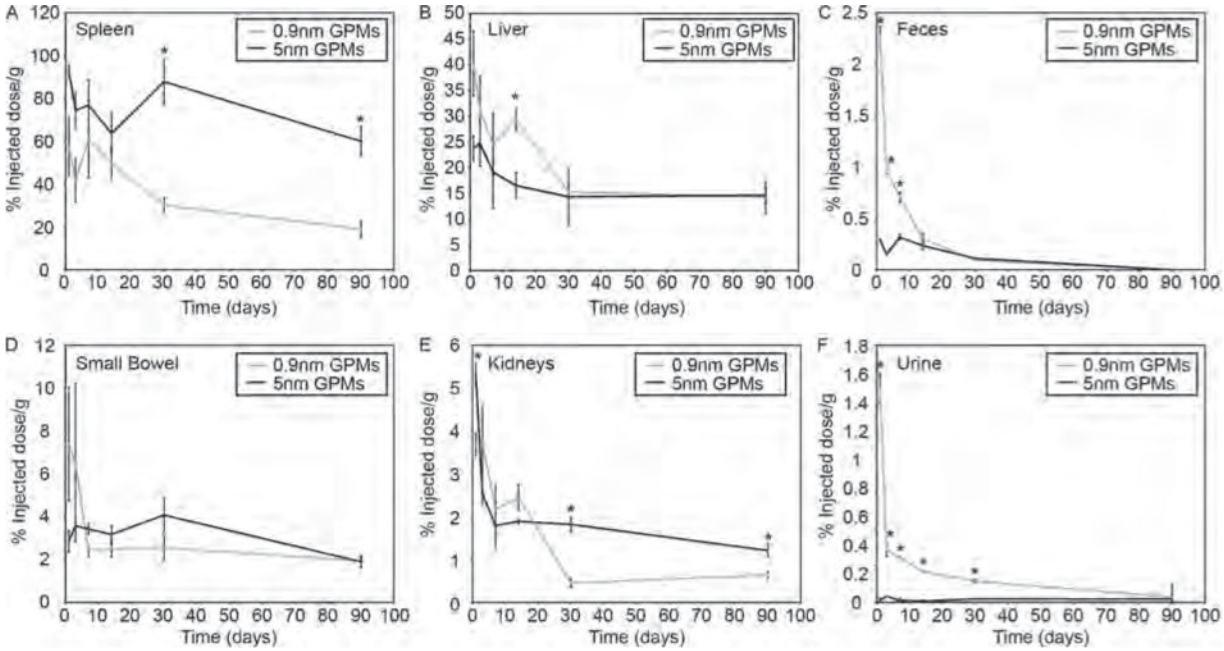


**Figure 4.**

Measurement of gold content in primary excretory organs and waste. The percent injected dose of gold per gram of tissue was measured in the (A) spleen, (B) liver, (C) feces, (D) small bowel, (E) kidneys and (F) urine at various times following the intravenous administration of 0.9 nm and 5 nm GPMs. All measurements of gold were acquired via ICP-OES. Asterisk indicates statistical significance ($p < 0.05$) between 0.9 nm GPM and 5 nm GPM groups.

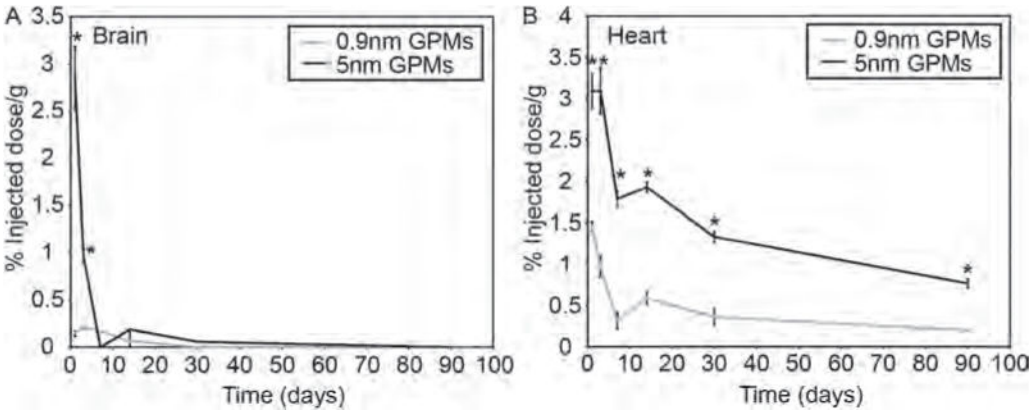


**Figure 5.**

Measurement of gold content in the brain and heart. The percent injected dose of gold per gram of tissue was measured in the (A) brain and (B) heart at various times following the intravenous administration of 0.9 nm and 5 nm GPMs. All measurements of gold were acquired via ICP-OES. Asterisk indicates statistical significance ($p < 0.05$) between 0.9 nm GPM and 5 nm GPM groups.

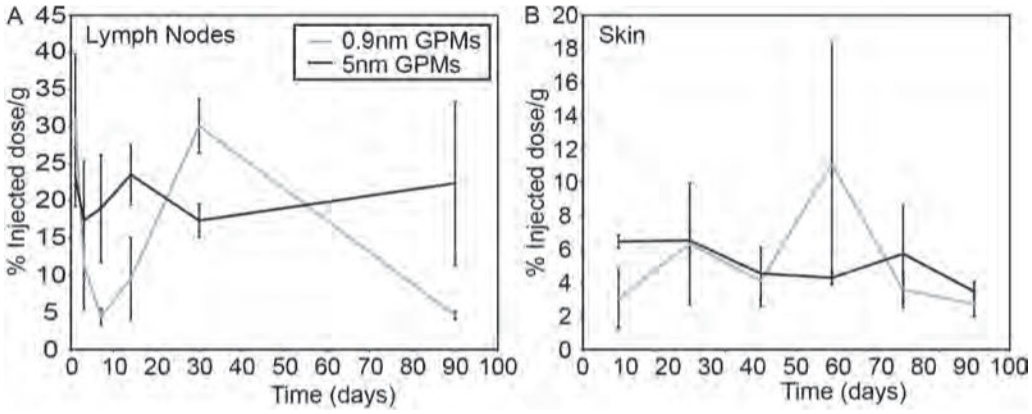


**Figure 6.**

Measurement of gold content in the lymph nodes and skin. The percent injected dose of gold per gram of tissue was measured in the (A) lymph nodes and (B) skin at various times following the intravenous administration of 0.9 nm and 5 nm GPMs. All measurements of gold were acquired via ICP-OES. No statistically significant difference ($p < 0.05$) was observed between 0.9 nm and 5 nm GPM groups.

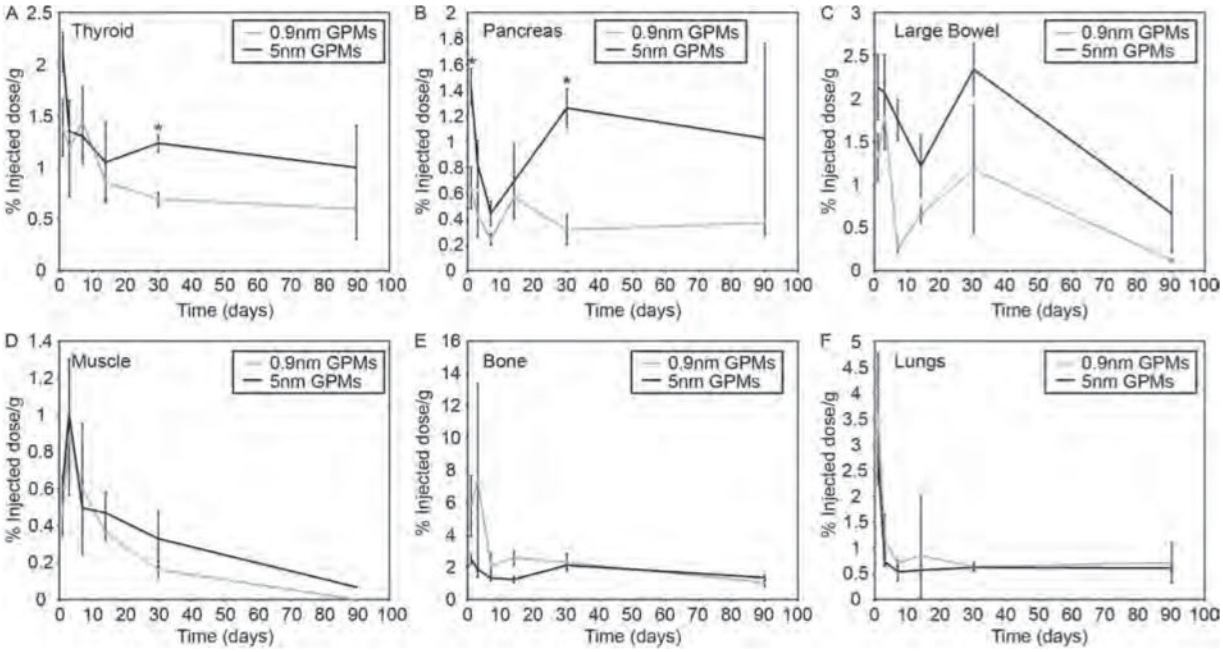


**Figure 7.**

Measurement of gold content in various organs. The percent injected dose of gold per gram of tissue was measured in the (A) thyroid, (B) pancreas, (C) large bowel, (D) muscle, (E) bone and (F) lungs at various times following the intravenous administration of 0.9 nm and 5 nm GPMs. All measurements of gold were acquired via ICP-OES. Asterisk indicates statistical significance ($p < 0.05$) between 0.9 nm GPM and 5 nm GPM groups.

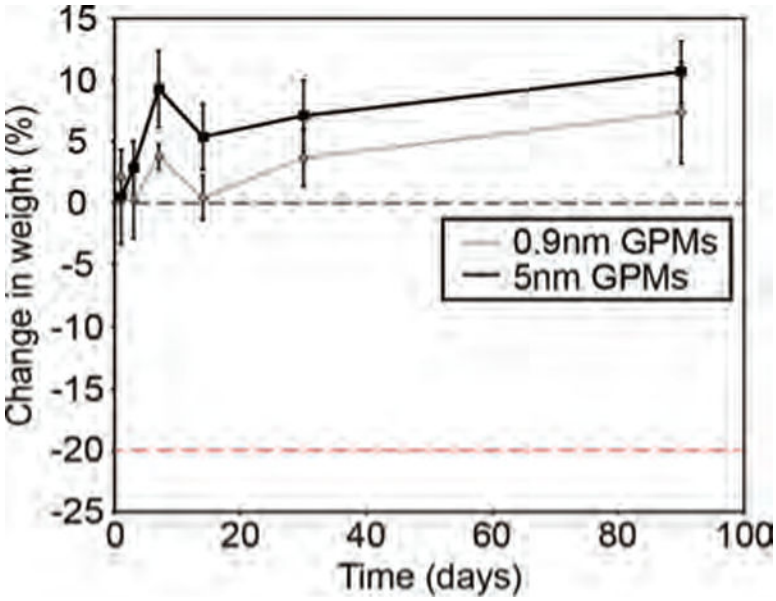


**Figure 8.**

Whole animal weights of mice treated with 0.9 nm or 5 nm GPMs (150 mg Au/kg). Data reflect average weights ($n = 3$) for each group.

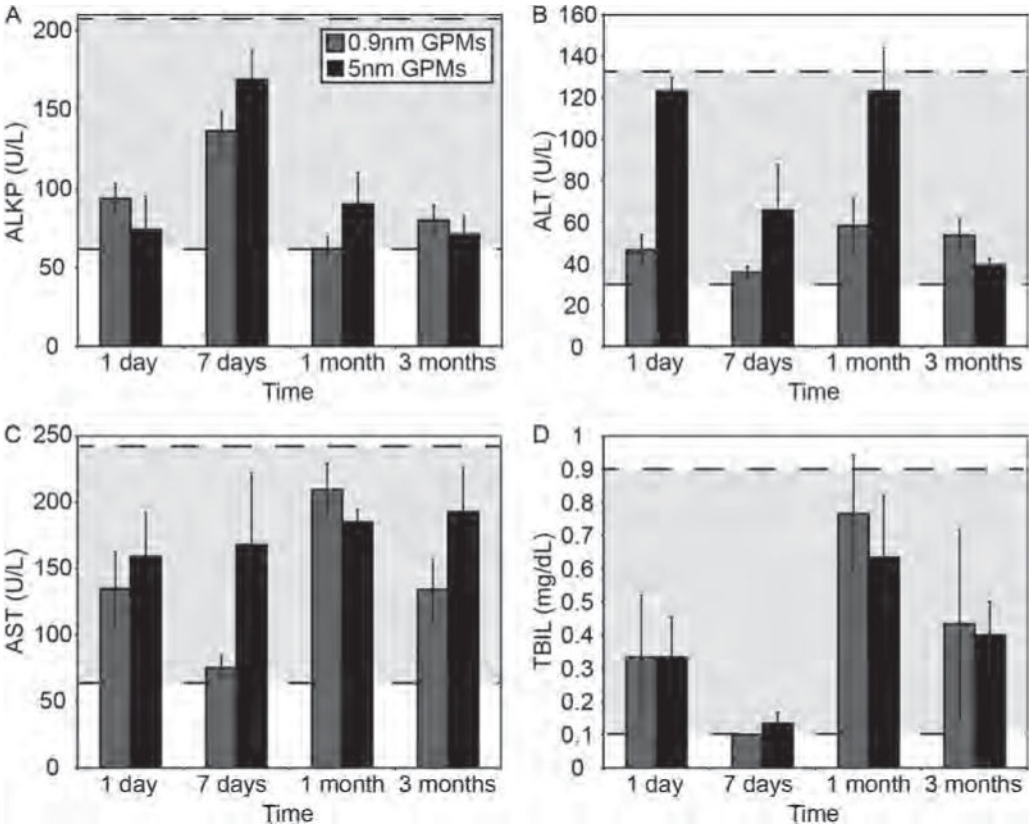


**Figure 9.**

Hematological analysis of mice treated with GPMs. Blood enzyme levels of female nude athymic mice were acquired 1 day, 7 days, 1 month, and 3 months days post-injection of 150 mg Au/kg of 0.9 nm GPMs (grey) or 5 nm GPM (black). Grey dotted lines denote the "normal" analyte levels. The specific enzymes analyzed were (A) alkaline phosphatase (ALKP), (B) alanine transaminase (ALT), (C) aspartate aminotransferase (AST), and (D) total bilirubin (TBIL).

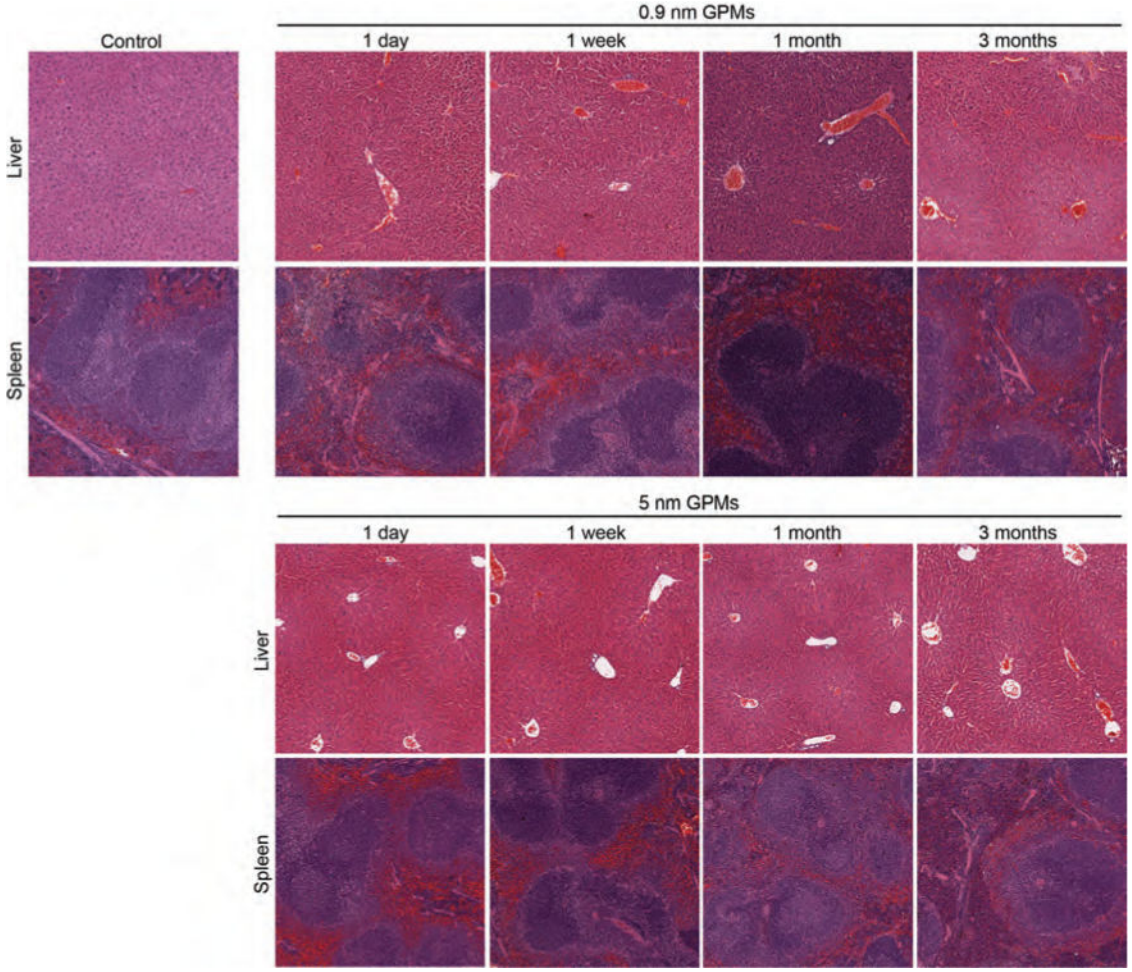


**Figure 10.**

Histological of liver and spleen for mice treated with GPMs. Mice ($n$ = 3 per group) received a single intravenous injection of 0.2 mL of either PBS (control), 0.9 nm GPMs, or 5 nm GPMs (150 mg Au/kg dose in PBS) followed by dissection of the liver and spleen at the indicated times. Sections were stained with H&E and images were acquired via light microscopy at 10× magnification.

**Table I**

GPM physical-chemical properties.

| AuNP size (nm) | Hydrodynamic diameter (nm) | Polydispersity index | Zeta potential (mV) |
|---|---|---|---|
| 0.93±0.19 | 79.8±3.9 | 0.083 | −1.50±1.10 |
| 4.66±0.57 | 78.5±2.4 | 0.075 | −1.04±0.84 |